Eur Biophys J (2014) 43:11–23
DOI 10.1007/s00249-013-0935-8

ORIGINAL PAPER

EBSA
Biophysics in Europe

Active contractions in single suspended epithelial cells

Markus Gyger · Roland Stange · Tobias R. Kießling · Anatol Fritsch · Katja B. Kostelnik · Annette G. Beck-Sickinger · Mareike Zink · Josef A. Käs

Received: 16 July 2013 / Revised: 8 October 2013 / Accepted: 15 October 2013 / Published online: 7 November 2013

Abstract Investigations of active contractions in tissue cells to date have been focused on cells that exert forces via adhesion sites to substrates or to other cells. In this study we show that also suspended epithelial cells exhibit contractility, revealing that contractions can occur independently of focal adhesions. We employ the Optical Stretcher to measure adhesion-independent mechanical properties of an epithelial cell line transfected with a heat-sensitive cation channel. During stretching the heat transferred to the ion channel causes a pronounced Ca^{2+} influx through the plasma membrane that can be blocked by adequate drugs. This way the contractile forces in suspended cells are shown to be partially triggered by Ca^{2+} signaling. A phenomenological mathematical model is presented, incorporating a term accounting for the active stress exerted by the cell, which is both necessary and sufficient to describe the observed increase in strain when the Ca^{2+} influx is blocked. The median and the shape of the strain distributions depend on the activity of the cells. Hence, it is unlikely that they can be described by a simple Gaussian or log normal distribution, but depend on specific cellular properties such as active contractions. Our results underline the importance of considering activity when measuring cellular mechanical properties even in the absence of measurable contractions. Thus, the presented method to quantify active contractions of suspended cells offers new perspectives for a better understanding of cellular force generation with possible implications for medical diagnosis and therapy.

Keywords Active soft matter · Epithelial contractions · Calcium · Optical Stretcher · Cell rheology

Electronic supplementary material The online version of this article (doi:10.1007/s00249-013-0935-8) contains supplementary material, which is available to authorized users.

M. Gyger (✉) · R. Stange · T. R. Kießling · A. Fritsch · M. Zink · J. A. Käs
Abteilung für Physik der weichen Materie, Institut für Experimentelle Physik I, Universität Leipzig, Linnéstr. 5, 04103 Leipzig, Germany
e-mail: markus.gyger@uni-leipzig.de

K. B. Kostelnik · A. G. Beck-Sickinger
Institut für Biochemie, Universität Leipzig, Brüderstr. 34, 04103 Leipzig, Germany

Introduction

Biological cells proliferate and migrate, they exert traction forces, and show contractile behavior in wound healing, embryonic development and many other processes. Their mechanical properties are mainly determined by the cytoskeleton, cytoskeletal cross-linkers and motor proteins (Lodish 2000). Cellular forces can be generated by motor activity (Vicente-Manzanares et al. 2009), polymerization (Mogilner and Oster 2003) and depolymerization (Sun et al. 2010). Active processes, such as exertion of forces via focal adhesions (Pelham and Wang 1999; Munevar et al. 2001; Ridley et al. 2003), response to changes in mechanical properties of the environment (Lo et al. 2000; Yeung et al. 2005), cell migration (Ridley et al. 2003; Wei et al. 2009; Friedl and Gilmour 2009) and actin treadmilling in lamellipodia (Ridley et al. 2003; Mogilner and Keren 2009), are performed under the consumption of energy provided by ATP. Hence, from a physical point of view, cells are active soft matter that exists in a thermodynamic state far from equilibrium (Cates and MacKintosh 2011).

To understand the underlying processes of cytoskeletal mechanics, reconstituted systems have been designed

consisting of a minimal number of elements, mostly actin filaments, myosin motors and passive cross-linkers. These approaches show that the fluctuation dissipation theorem is violated in such systems (Mizuno et al. 2007). Systems consisting of actin filaments, cross-linkers, and active myosin motors allow reproducing several of the non-linear effects that are observed in cells such as stress stiffening (Mizuno et al. 2007) and contractions (Bendix et al. 2008). On the other hand, bottom-up theoretical approaches built on the a priori assumption that motor-induced contractility provides the force-inducing effect in active gels are able to explain stress stiffening (MacKintosh and Levine 2008) and also macroscopic contractions (Liverpool et al. 2009).

Contractions are a vital feature of physiologically relevant processes in a variety of cells. Non-muscle myosin produces traction forces in fibroblasts (Beningo et al. 2006; Lo et al. 2004; Mader et al. 2007). Epithelial contractions play a role in wound healing (Tamada et al. 2007; Bement et al. 1993) and embryonic development (Jacinto et al. 2000; Martin et al. 2009). There are indications that the ability to actively contract correlates with tumor progression and metastatic potential (Mierke et al. 2008; Fritsch et al. 2010; Jonas et al. 2011). Understanding of contraction mechanisms and pathways might provide a target in cancer therapy. Thus, identification and analysis of contractile cells are important tasks to understand the fundamentals of cell functioning and may provide a vital basis for the development of new therapeutic approaches.

To date, a number of experiments have been performed interpreting cellular mechanics by passive material properties (Yamada et al. 2000; Fabry et al. 2001; Wottawah et al. 2005a, b; Icard-Arcizet et al. 2008; Maloney et al. 2010). In these experiments broad distributions in mechanical properties, such as the elastic modulus, have been observed (Guck et al. 2005; Hoffman et al. 2006), while it remains unclear how they can be described mathematically. There is striking evidence that the mechanics of adherent cells follows a power law in rheology (Yamada et al. 2000; Fabry et al. 2001; Icard-Arcizet et al. 2008; Desprat et al. 2005). Non-linear elasticity effects, such as fluidization and stress stiffening in adherent cells, have been shown to be linked to power-law rheology by cytoskeletal pre-stress (Kollmannsberger et al. 2011; Stamenovic et al. 2004). Experiments on single suspended cells measured by optical stretching so far seemed to be an exception to power-law rheology (Wottawah et al. 2005a, b); however, the discussion is still ongoing (Maloney et al. 2010).

Active forces within the cytoskeleton of living cells have been investigated with microrheology (Lau et al. 2003). At large deformations, a building up of contractile forces within several tenths of minutes have been shown by microplate rheology (Thoumine and Ott 1997). Cells held at a constant elongation between the microplates generate a contractile traction force within several hundreds of seconds involving shape changes from convex to concave shape (Mitrossilis et al. 2009). These measurements were performed with cells adhered to stiff substrates. On deformable substrates, traction forces of adhered cells could be measured (Munevar et al. 2001; Beningo et al. 2006; Lo et al. 2004; Mader et al. 2007; Wang et al. 2001a).

The main candidate for causing contractions is myosin, which can be activated by Ca^{2+} via the myosin light-chain kinase pathway (Fukata et al. 2001; Somlyo and Somlyo 2003). Also other mechanisms that can lead to contractions depend on calcium: Ca^{2+} regulates several actin-modifying proteins (Walsh et al. 1984; Kumar et al. 2004; Larson et al. 2005) and was shown to influence microtubule depolymerization (Salmon and Segall 1980).

In this work, we present for the first time that fast contractions, i.e., within a few seconds, happen in epithelial cells without involvement of focal adhesion-dependent processes. The Microfluidic Optical Stretcher (μOS) allows measuring adhesion-independent cellular mechanics (Guck et al. 2005; Lincoln et al. 2007; Remmerbach et al. 2009). Using the μOS, we are able to observe contractions of fully suspended cells. Furthermore, we elucidate the influence of Ca^{2+} signals on these contractions. To this end, the wild-type epithelial cell line HEK293 (HEK293-wt) and the same cell line stably transfected with the heat-activated transient receptor potential cation channel subfamily member vanilloid 1 (HEK293-TRPV1) (Caterina et al. 1997; Tominaga et al. 1998) are used. The μOS measurement provides sufficient heat to open the TRPV1 channels and triggers a massive Ca^{2+} influx that can be inhibited by the application of channel blockers and Ca^{2+} chelators, constituting a cellular system with a tunable switch for controlling the Ca^{2+} entry. The μOS is thus an ideal tool to measure the Ca^{2+}-dependent mechanical properties of the HEK293-TRPV1 cells (Gyger et al. 2011). This way, the calcium signal in the HEK293-TRPV1 cells can be manipulated, providing a good model system for the investigation of the influence of Ca^{2+} on the cell mechanics.

In our experiments several of the measured HEK293-TRPV1 and HEK293-wt cells show contractions against the applied external stress. By inhibition of the calcium influx in HEK293-TRPV1, the strain can be changed significantly, indicating an influence of the second messenger Ca^{2+} in the generation of the observed cellular forces. Blocking the Ca^{2+}-dependent myosin activation pathway with ML-7 reduces the number of contractile cells and the strength of the contractions, but does not inhibit these contractions completely. This observation suggests that Ca^{2+}-activated myosin motor activity is involved in the contraction process. However, it is not the only mechanism responsible for the measured contractions of suspended epithelial cells.

The observed cellular behavior shows that a description of cellular mechanics requires the identification of a leading term in active cellular contractions. To this end, a phenomenological mathematical model is derived from the general constitutive equation for linear viscoelastic materials (Tschoegl 1989), including a leading term of active force generation by the cell. It turns out that active cellular contractions are sufficient to explain the differences in deformations of cells with and without Ca^{2+} influx. Despite its simplicity, our model provides a powerful method to quantify active contractions of the investigated cells. Furthermore, it allows an unbiased view on the contractions without a priori assumptions on force-generating mechanisms. Combining creep rheology measurements in the -μOS with a phenomenological description, our results provide new insight into non-muscular force generation and cellular adaptation to environmental stimuli. We show for the first time fast contractions in suspended epithelial cells, i.e., without the involvement of focal adhesion complexes or other attachments to their surrounding.

Experimental

Optical stretching and image analysis

The Microfluidic Optical Stretcher setup is built as described in (Gyger et al. 2011; Lincoln et al. 2007). Cells are moved into the trap region by controlling the pressure with custom-made pumps. After stopping the flow, the cells are trapped at 0.1 W per fiber with two counter propagating beams emerging from two 1,064 nm single mode CW ytterbium fiber lasers (YLM-5-SC, IPG Laser GmbH, Burbach, Germany) equipped with a beam splitter. Cells are stretched at 0.7 W per fiber for 5 s followed by a relaxation phase at trapping power for 2 s. Phase contrast images at 63× magnification are recorded at 30 fps with an A622f (Basler, Ahrensburg, Germany) camera mounted on an Axiovert 40c microscope (Zeiss, Oberkochen, Germany). The laser is controlled via custom-written Labview (National Instruments, Austin, Texas) software. The cell edge is detected for every frame from the phase contrast images using custom-written Matlab (The MathWorks Inc., Natick, MA, USA) software. The strain, defined as the change of the length of the cell's axis along the laser beam during the stretch phase divided by the diameter of the unstretched cell, is calculated.

Cell culture

Human embryonic kidney cells (HEK293), stably transfected with the TRPV1 ion channel, were kindly provided by David Julius, University of California, San Francisco (UCSF). As has been shown previously (Gyger et al. 2011), the μOS triggers a Ca^{2+} signal by activation of the TRPV1 ion channel. The cells are cultured and detached as described in (Gyger et al. 2011). HEK293 wild-type cells are cultured under the same conditions, without the selective antibiotic G418 disulphate. All measurements are performed with cells suspended in a calcium imaging buffer (CIB) consisting of 6 mM KCl (Roth, Karlsruhe, Germany), 134 mM NaCl, 1 mM $MgCl_2$, 2.5 mM $CaCl_2$, 10 mM p-(+)-glucose and 10 mM Hepes (all from Sigma-Aldrich, St. Louis, MO). The pH is adjusted to 7.45 with NaOH (Sigma-Aldrich). For Ca^{2+}-free measurements a calcium-free imaging buffer (CfIB) is used, replacing the $CaCl_2$ by 10 μM EGTA (Fluka/Sigma-Aldrich, St. Louis, MO).

Drug application

The Ca^{2+} chelator BAPTA,AM (PromoCell, Heidelberg, Germany) competitively binds Ca^{2+} ions inside the cell. The messenger Ca^{2+} is hindered from interacting with its natural binding partners such as receptors and pumps; hence, the signal cascade is interrupted. BAPTA is loaded into the cells as described in (Gyger et al. 2011) using the acetoxymethyl ester form, a membrane-permeable molecule, which is de-esterified by intracellular esterases, activating it and making it membrane impermeable. The suspended cells are incubated for 15 min in 1 ml phosphate buffer saline solution (PBS, Invitrogen Corp., Carlsbad, CA) containing 20 μM BAPTA-AM; 7.7 μl of a pluronic F127 solution in 20 % DMSO (PromoCell, Heidelberg, Germany) is added to facilitate chelator loading and avoid compartmentalization. The TRPV1 channel is blocked by 10 μM ruthenium red (RuR, Sigma-Aldrich, St. Louis, MO). Control experiments testing for the involvement of stretch-activated Ca^{2+} channels (SACs) are performed with 10 μM $GdCl_3$ (Sigma-Aldrich, St. Louis, MO). In these experiments RuR respectively $GdCl_3$ is added to the cell culture medium during Optical Stretcher measurements.

ML-7 blocks MLCK with a K_i value of 0.3 μM (Saitoh et al. 1987). It interrupts the Ca^{2+}-dependent myosin motor activation pathway. To assure MLCK blocking, 1 μM ML-7 was added to the cell culture flask of attached cells 6 h prior to the experiments and was also present during the measurements.

Results

Ca^{2+} influences cellular contraction in suspended epithelial cells

In the μOS suspended cells are trapped and stretched by two counterpropagating laser beams. The lasers exert a

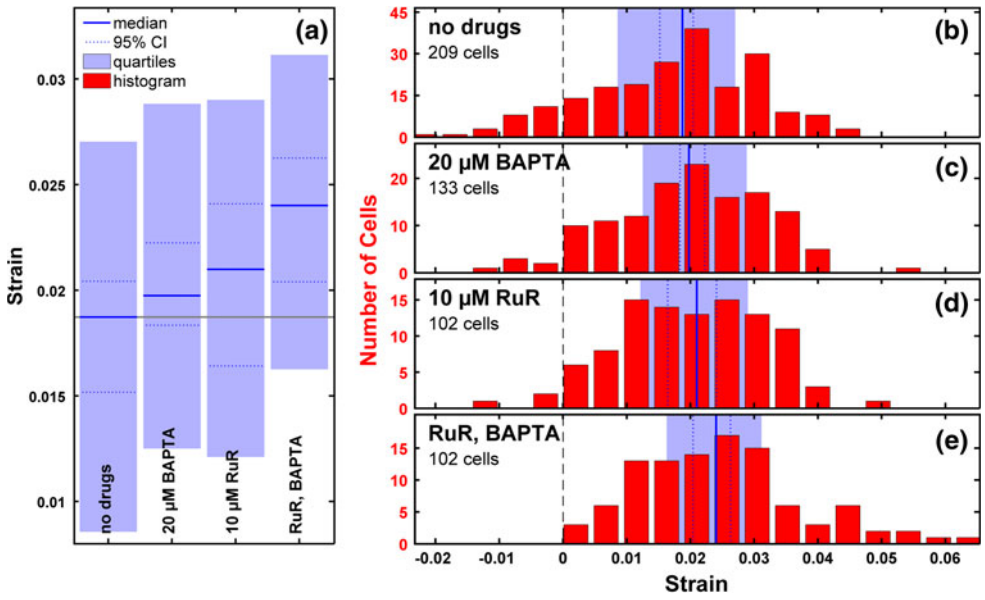

Fig. 1 Strain distributions of HEK293-TRPV1 cells in the µOS after 5 s of stretch with 0.7 W: median (*blue line*) of each of the µOS measurements with 95 % confidence interval (CI) calculated with the bootstrap method (*dotted blue line*) and quartiles (*light blue area*). **a** Overview: the *gray line* indicates the median of the experiment with untreated HEK293-TRPV1 cells. If a median is outside the 95 % CI of the other distribution, the probability that the medians are different is larger than 95 %. **b–e** Histograms (*red*) of the distributions of strains after 5 s stretch. The *dashed black line* marks the zero strain, i.e., strains below this value indicate contractions that deform the cell below its original elongation. Blocking the Ca^{2+} influx through the TRPV1 channel with RuR and chelating the remaining Ca^{2+} with BAPTA increases the strain as contractions are less pronounced (**c–e**)

stress normal to the cell surface. A contractile force of the cell would act against this externally applied force. If the overall force per unit area of the cell on its surface overcomes the external stress, the cell contracts, i.e., the cell's half axis parallel to the direction of laser light propagation shrinks. HEK293 wild-type cells (HEK293-wt) and HEK293 cells transfected with the heat-activated TRPV1 channel (HEK293-TRPV1) are measured in the µOS for 5 s at 0.7 W per fiber. The strain of the cells along the direction of laser propagation is determined by optical video microscopy.

The Ca^{2+} signal in HEK293-TRPV1 cells can be blocked almost completely using a combination of 20 µM BAPTA-AM and 10 µM RuR (Gyger et al. 2011). RuR blocks the Ca^{2+} entry through the TRPV1 channels, and the chelator BAPTA competitively binds internal Ca^{2+} ions. At a concentration of 10 µM RuR, the inward current through the TRPV1 channels is reduced by 90 % (Caterina et al. 1997, 1999). Our experiments show that the cellular strain increases with decreasing Ca^{2+} influx. Measured strain distributions after a step stress of 5 s are given in Fig. 1 for HEK293-TRPV1 cells and for HEK293-wt cells in Fig. 2. Figure 1a shows the medians of the strain distribution with 95 % confidence intervals (CI) and quartiles. As the type of distribution is unknown, the CI is calculated with the bootstrap method (Efron and Tibshirani 1994). In the bootstrapping algorithm the measured distribution is assumed to be the correct one. The desired statistical quantity, in this case the CI, is then calculated from a given number of artificial data sets, generated such that they follow the assumed distribution.

While the application of the chelator BAPTA to HEK293-TRPV1 cells has a small, insignificant effect on the strain, blocking the channel with RuR already results in larger deformations. The median of strain of the HEK293-TRPV1 cells treated with both RuR and BAPTA lies outside the 95 % CI of the median from untreated cells and vice versa, indicating a probability of more than 95 % that the distributions differ. Furthermore, the addition of RuR and BAPTA changes the skewness of the distribution: the strain distribution of the untreated (high Ca^{2+}) cells has a long tail to the left reaching below zero, i.e., the cells exhibit pronounced contractions (Fig. 1b). HEK293-TRPV1 cells with low Ca^{2+} influx show a rather symmetric strain distribution with only a few strongly contracting cells (Fig. 1c, d). For HEK293-TRPV1 cells with almost complete blockage of the Ca^{2+} signal, the skewness is positive, a long tail to large deformations becomes visible, and no contractions below the initial elongation occur (Fig. 1e). Videos of a strongly contracting and a passively elongating HEK293-TRPV1 cell can be found in Video S1 and Video S2 in the ESM.

Fig. 2 shows the distributions of deformations for HEK293-wt cells. For all three measurements, it is visible that for a subset of the cells the overall strain is negative, i.e., the elongation after the optical stretching is smaller than before the measurement–the cell strongly contracts.

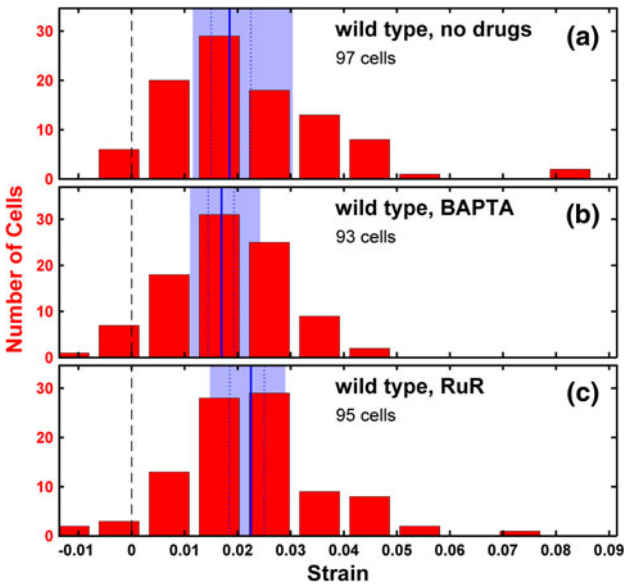

Fig. 2 Strain distributions (*red*) of HEK293-wt after 5 s optical stretching at 0.7 W: median (*blue line*) of each of the μOS measurements with 95 % CI calculated with the bootstrap method (*dotted blue line*) and quartiles (*light blue area*). **a** Untreated, **b** treated with 20 μM BAPTA,AM to chelate internal Ca^{2+} signaling, and **c** treated with 10 μM RuR to test whether the substance itself has an effect on cellular activity. In all three cases, a few cells show strong contractions with a final negative strain (*dashed black line* marks zero strain). While there seems to be a small difference in strain between the BAPTA-treated (**b**) and RuR-treated cells (**c**), neither BAPTA nor RuR treatment results in a significant difference in strain compared to untreated HEK293 wild-type cells, confirming the interpretation that Ca^{2+} influx through the TRPV1 channel in HEK293-TRPV1 cells influences the observed contractions

A significant influence of the chalator BAPTA was not visible in HEK293-wt cells (Fig. 2b). Figure 2c shows that the strain distribution is not changed significantly when 10 μM RuR is applied to HEK293-wt cells, confirming that the TRPV1 channel blocker does not produce any unwanted side effects. These observations confirm the assumption that the massive influx through the TRPV1 channel triggered by optical stretching (Gyger et al. 2011) influences the contractions as a downstream effect.

In order to test whether Ca^{2+} entry through stretch-activated channels (SAC) has an influence on the observed contractions, Gd^{3+} ions, a known blocker of SAC, are applied during the experiments. Experiments performed in a solution of 10 μM $GdCl_3$ do not result in a significant change of the strain distribution, neither for HEK293-TRPV1 cells (Fig. S1a,b in the ESM) nor for untransfected HEK293-wt cells (Fig. S5a,b in the ESM). This finding indicates that Ca^{2+} entry through SAC does not have a significant influence on the observed contractions.

In a control experiment with the amount of DMSO as used for the BAPTA experiment, the cellular strain in HEK293-TRPV1 cells does not significantly change compared to the untreated cells (Fig. S1a,c in the ESM). Optical stretching in Ca^{2+}-free imaging buffer (CfIB) results in partial suppression of the contractions similar to that observed in RuR-treated cells (Fig. S1d in the ESM). However, the overall strain of the cells in this control experiment is slightly lower than for cells in Ca^{2+} imaging buffer (CIB). This difference is most likely caused by a slightly changed osmolarity due to the lack of Ca^{2+} ions.

If the contractions in HEK293-TRPV1 cells were caused solely by Ca^{2+}-dependent myosin activation, blocking Ca^{2+} signals and directly interrupting the pathway at the MLCK level should have similar effects. On the other hand, an additional blocking of Ca^{2+} should not further influence the strain, as the pathway is already inactive. To test for this hypothesis, we blocked the MLCK with 1 μM ML-7. The result can be seen in Fig. S2 in the ESM. The median of strain from the ML-7 experiments (Fig. S2e in the ESM) does not differ significantly from the median of the measurements with blocked Ca^{2+} by BAPTA and RuR (Fig. S2d in the ESM). The strain distribution for the ML-7 experiments becomes almost symmetric (Fig. S2e in the ESM) and still shows strong contractions that lead to strains below zero; contractions are hence not hindered completely by MLCK blocking. Applying the same amount of ML-7 to the HEK293 wild-type cells does not lead to significantly larger strains, indicating that this effect depends on the influx of external Ca^{2+}.

A co-application of Ca^{2+} blocking and ML-7 showed that the increase of strain caused by Ca^{2+} influx and that due to MLCK-blocking are to some extent independent (Fig. S2e–g in the ESM). Taken together, our findings indicate that the observed contractions are caused in part by myosin contractility via the MLCK pathway and in part by a different mechanism unaffected by ML-7.

Model derivation and fitting

To elucidate the influence of active processes on the mechanical properties of the investigated cells, we present a descriptive model including active contractions of the cell upon optical stretching. To this end, the ansatz from Wottawah et al. (2005a, b) is extended by a term representing an active force exerted by the cell on its surface. Solving the general constitutive equation, an analytic description of the strain in the μOS is obtained. A detailed derivation can be found in Text S1 in the ESM.

The equation linking time-dependent stress $\gamma(t)$ and strain $\sigma(t)$ of a linear viscoelastic material is given by the general constitutive equation with constant coefficients a_m and b_n (Tschoegl 1989):

$$\sum_{m=0}^{\infty} a_m \frac{\mathrm{d}^m \gamma(t)}{\mathrm{d}t^m} = \sum_{n=0}^{\infty} b_n \frac{\mathrm{d}^n \sigma(t)}{\mathrm{d}t^n}. \quad (1)$$

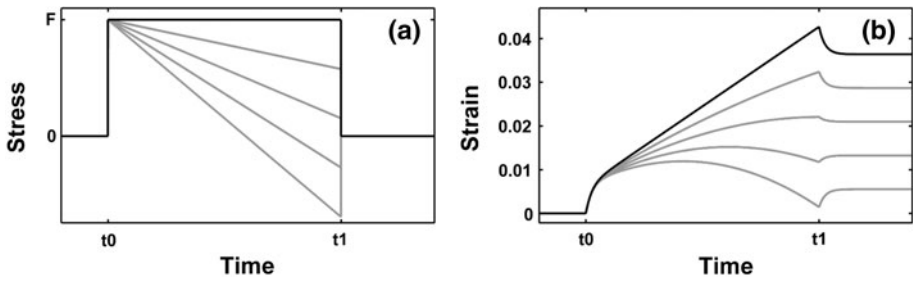

Fig. 3 Modeled stress and strain over time for different values of the activity parameter A. The parameters a_1, a_2 and b_1 are set to the median obtained from the measurements of all untreated cells. **a** Step stress exerted by the μOS (*black*) and sum of stresses exerted on the cell surface (*gray*) as described in Eq. (3) for A/Pa s^{-1} = 1.0, 2.0, 3.0, 4.0. For high A the stress on the cell surface becomes negative. **b** The resulting cellular strain calculated with Eqs. (4) and 5. For higher activities the strain decreases. Negative slopes of the graph indicate visible contractions

Following the arguments of Park and Schapery (1999) a sufficiently good description is given by:

$$a_1 \frac{\mathrm{d}\gamma(t)}{\mathrm{d}t} + a_2 \frac{\mathrm{d}^2\gamma(t)}{\mathrm{d}t^2} = \sigma(t) + b_1 \frac{\mathrm{d}\sigma(t)}{\mathrm{d}t}. \tag{2}$$

The stress $\sigma(t)$ exerted on the cell surface by the μOS can be described by a rectangular function. Assuming the trapping forces to be small, the stress is set to zero at $t < 0$ and at $t > t_1$. We further assume that the stress $\sigma_{\mathrm{cell}}(t)$ exerted by active cellular forces on the surface is zero at zero external stress, i.e., at $t < 0$ and at $t > t_1$. For the interval $0 > t > t_1$, $\sigma_{\mathrm{cell}}(t)$ can be represented as the multiplication of $[\Theta(t) - \Theta(t - t_1)]$ and a Taylor expansion of a stress term defined on the interval $[-\infty, \infty]$. As there is no initial active cellular stress, the zeroth order in the resulting Taylor expansion vanishes. Including the terms up to the fist order, the total stress can be described by (Fig. 3a):

$$\begin{aligned}\sigma(t) &= \sigma_{\mathrm{laser}}(t) + \sigma_{\mathrm{cell}}(t) \\ &= (F_{\mathrm{G}}\sigma_0 - A \cdot t) \cdot [\Theta(t) - \Theta(t - t_1)],\end{aligned} \tag{3}$$

where F_{G} is the geometric factor, a constant accounting for the geometry of the trapped cell, and σ_0 is the peak stress in direction of the laser axis (Wottawah et al. 2005a, b). A is the activity parameter characterizing the first order approximation of contractile cellular stresses.

Setting $F := F_G\,\sigma_0$ and applying the boundary conditions $\gamma_1(t) := \gamma(t<0) = 0$ and $\sigma(t < 0) = 0$, this differential equation can be solved. For $0 < t < t_1$ we have:

$$\begin{aligned}\gamma_{\mathrm{II}}(t) = -\frac{1}{a_1^3}\Bigg[&\left(\exp\left\{-\frac{a_1}{a_2}t\right\} - 1\right) \cdot \left(Aa_2^2 \right. \\ &\left. - Aa_1a_2b_1 + a_1a_2F - a_1^2b_1F\right) \\ &+ t\left(Aa_1a_2 - Aa_1^2b_1 + a_1^2F - \frac{1}{2}Aa_1^2t\right)\Bigg],\end{aligned} \tag{4}$$

and for $t > t_1$:

$$\begin{aligned}\gamma_{\mathrm{III}}(t) = +\frac{1}{a_1^3}\Bigg[&\exp\left\{-\frac{a_1}{a_2}t\right\}\left(Aa_2^2 - Aa_1a_2b_1 + a_1a_2F \right. \\ &\left. - a_1^2b_1F\right) - \exp\left\{-\frac{a_1}{a_2}(t - t_1)\right\}\left(Aa_2^2 \right. \\ &- Aa_1a_2b_1 + a_1a_2F - a_1^2b_1F - Aa_1a_2t_1 \\ &\left. + Aa_1^2b_1t_1\right) + a_1^2Ft_1 - \frac{1}{2}Aa_1^2t_1^2\Bigg].\end{aligned} \tag{5}$$

The shape of $\gamma(t)$ with typical parameters can be seen in Fig. 3b. Increasing the activity parameter A results in a decrease of the strain and for high A values even in visible contractions, i.e., a strain with negative slope.

The mathematical description of the relaxation phase (Eq. 5) follows from the assumption that the stress exerted by the cell ceases immediately as soon as the external stress falls back to zero. In fact, this is the description of a passively relaxing material. If the total deformation is a contraction below the initial elongation, one would expect an expansion after the step stress, as shown in the lowest two graphs in Fig. 3b. The example of such a strongly contracting cell, shown in the lowest graph in Fig. 4, demonstrates that this behavior is not observable in the measured cells. We therefore decided to fit only the measured strain for $0 < t < t_1$ ("stretch phase") with the model (Eq. 4) to obtain the parameter a_1, a_2, b_1 and A. The graphs for the time after the end of the stretch phase ("relaxation phase") shown in Fig. 4 are obtained by inserting these values into Eq. (5). The difference between the model prediction and the fit is obvious from the examples shown in Fig. 4. Instead of increasing, the strain stays almost constant or slightly continues to decrease, which proves that the relaxation is not entirely passive. Similar to the strain during the stretch phase, the relaxation phase is strongly influenced by active forces of the cell.

Fitting Eq. (4) to the strain data is performed using a nonlinear least square fitting algorithm of Matlab, weighted with the inverse square of the interquartile distance. This

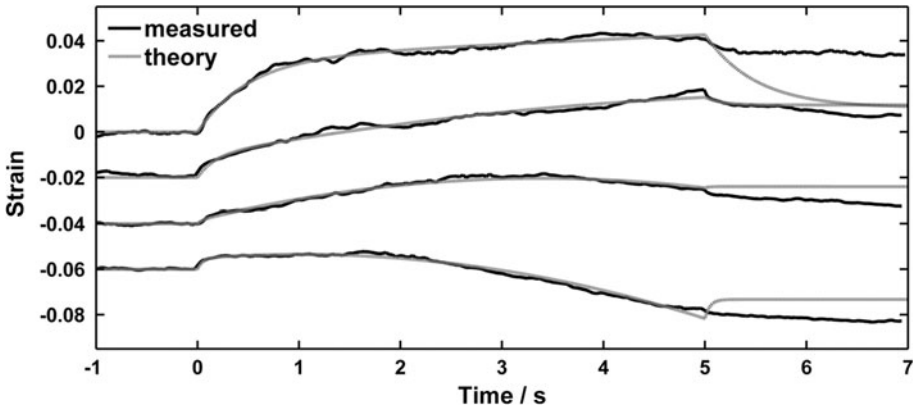

Fig. 4 Examples of fits of the model to the strain of untreated HEK293-TRPV1 cells with different values for the activity parameter A. From *top* to *bottom*: $A/\mathrm{Pa\,s^{-1}} = 0.0004, 1.55, 3.4,$ and 6.8. For $0 < t < t_1 = 5$ s, the model describes the measured strains well. For $t > 5$ s, the graph is plotted with the parameter set obtained from the fit for $0 < t < 5$ s. It becomes obvious that the deviations at $t > 5$ s are large for all cases, indicating that the assumption of a passively relaxing material fails

procedure resulted in more reliable fitting for small times. Larger differences between fit and measurements toward the end of the stretch ($t \lesssim t_1$) are caused by deviations from the assumption that the force exerted by the cells can be described well enough by a linear term.

Calculations of the geometric factor F_G require an exact knowledge of the thickness of the actin cortex, which provides the main contribution to the resistance to deformation (Wottawah et al. 2005a, b). The exact geometry of the cytoskeleton's compound structure can, however, not be determined. It is hence not possible to calculate a reliable geometric factor. We therefore decided to perform a parameter sweep on $F := F_G\,\sigma_0$. Fitting with F as an additional parameter is not an option since it depends on the fit parameters a_1 and a_2. Based on estimates of realistic values, obtained by the calculation proposed in (Ananthakrishnan et al. 2005), we tested F for values between 2.5 and 32 Pa while recording the median of the correlation coefficient r^2. The influence on the quality of the fits is negligible, as the other dependent parameters compensated for the deviations. Results of the parameter sweep can be seen in Fig. S3 in the ESM. The findings resulting from our model are thus independent of the choice of F, and the parameter can be fixed arbitrarily, if the model is applied to compare different experiments. Assuming a thickness of the actin cortex of 10 % of the cell radius and estimating the peak stress to be $\sigma_0 = (3.7 \pm 1.0)$ Pa, the parameter F is set to 11.8 Pa.

For some graphs the fit parameters diverge. We therefore restrict each of the parameters to a multiple of the median calculated from unrestricted fits. If one of the parameters reaches the boundary value or if the correlation coefficient r^2 is below 0.7, fitting is repeated using the robust fitting method of least absolute residuals (LAR). For the presented data this procedure recovers 17.1 % of the cells with r^2 below 0.7. Graphs that still diverge or have an r^2 below 0.7 are excluded from the analysis (11.5 %). Examples of the fit to measured strains are presented in Fig. 4. Reasons for the divergence in parameters are discussed in the section "Applicability of the model" of the "Discussion".

Activity parameter correlates with cellular contractions

The parameters a_1, a_2 and b_1, describing the passive behavior, and the activity parameter A are determined by fitting Eq. (4) to the strain of every measured cell. Figure 5 shows A for untreated HEK293-TRPV1 cells (a) and cells treated with 10 μM RuR and 20 μM BAPTA (b). Only approximately 18 % of the untreated HEK293-TRPV1 cells (Fig. 5a) and 22 % of the untransfected HEK293-wt cells (Fig. S6a in the ESM) are describable by a passive viscoelastic behavior, i.e., with an activity parameter $A \approx 0$. Blocking the Ca^{2+} signal in HEK293-TRPV1 cells, this fraction increased to approximately 29 %, and the number of highly active cells as well as the maximal activity decrease (Fig. 5b). (The distributions of the passive material properties are available in ESM Fig. S4).

In Figs. 5 and 6 as well as Fig. S4 in the ESM, it becomes obvious that the distributions are highly non-Gaussian; calculation of the mean value with standard error propagation therefore does not give reliable information about the significance of the differences in the measured quantities. To elucidate the significance of differences in the data, we calculated a 95 % CI with bootstrapping (Efron and Tibshirani 1994) and applied a Wilcoxon rank sum test (Mann and Whitney 1947). This test is a standard non-parametric test, checking for the hypothesis that one of the distributions tends to have larger values than the other. The test is positive if the p value is below 0.05. In this case

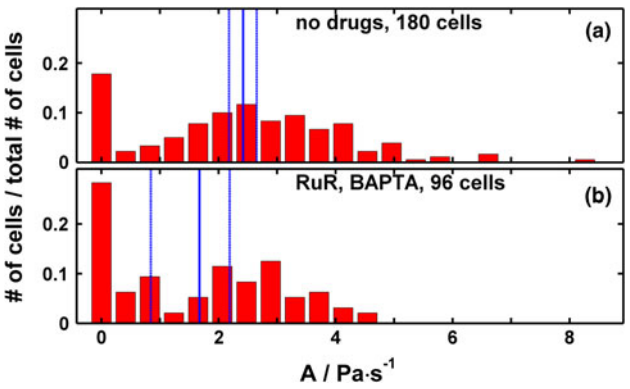

Fig. 5 Histogram of the activity parameter A normalized with the total number of measured cells in the experiment (*red*). The *solid blue line* indicates the median and the *dotted blue line* the 95 % confidence interval calculated with bootstrapping. **a** Untreated, **b** Ca^{2+} signaling blocked with 10 μM RuR and 20 μM BAPTA. While all other fit parameters do not differ (see Fig. S4 in the ESM), the distributions are distinguishable by the cell's active stress. The percentage of non-active cells ($A \approx 0$) is higher for the case where Ca^{2+} is blocked

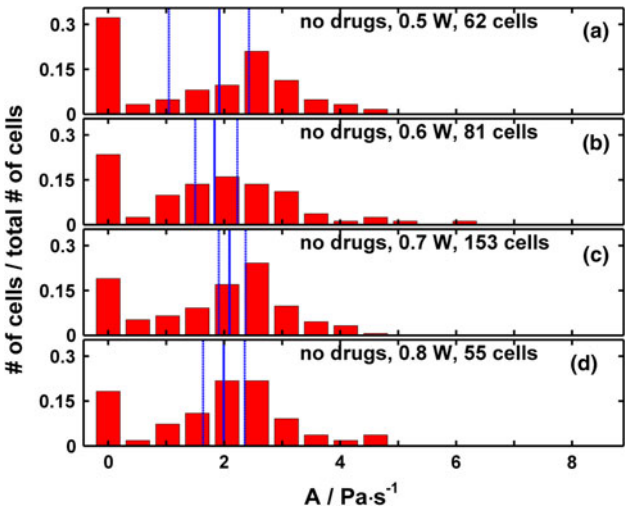

Fig. 6 Activity parameter A of HEK293-TRPV1 cells measured at laser powers between 0.5 and 0.8 W. The median of strain increases with laser power; hence, the fit parameters a_1, a_2 and b_1 vary. At 0.5 W, where TRPV1 channels are not opened (Gyger et al. 2011), the fraction of non-active cells ($A \approx 0$) is approximately 32 %. With increasing power, it drops down to roughly 16 %. This confirms the hypothesis that part of the contractile behavior but not all of it is triggered by the Ca^{2+} signal. On the other hand, it nicely shows that the presented model gives reliable results under altered boundary conditions

the probability for the hypothesis to be true is larger than 95 %. While Fig. 1 shows clear differences in the distributions of the whole cell strain, in none of these experiments is the rank sum test positive for the parameters a_1, a_2 or b_1. Hence, the treatment with Ca^{2+} influx-inhibiting drugs does not have a significant influence on the passive mechanical properties of the measured cells (Fig. S4 in the ESM). The difference between the distributions of the activity parameter A of the untreated case and the experiment with blocked Ca^{2+} signaling is clear ($p = 0.00088$, Fig. 5). The observed differences in strain are therefore explicable by differences in the active behavior of the cells.

When measuring HEK293-TRPV1 cells suspended in Ca^{2+}-free buffer, the median of A is lowered in a similar way to that in experiments where the TRPV1 channels is blocked by RuR (Fig. S5d in the ESM), supporting the hypothesis that the Ca^{2+} influx causes the observed change. However, the strain of cells measured in CfIB is significantly lower than for measurements in CIB. The reason for this effect is most likely a different osmolarity due to the lack of Ca^{2+} ions (Fig. S1 in the ESM). As expected, Ca^{2+} signal chelation by BAPTA does not have a significant effect on the activity in wild-type cells (Fig. S6a, b in the ESM). Applying RuR to wild-type cells does not reveal any change in the activity either (Fig. S6c in the ESM), confirming that the influence of RuR solely originates from channel blockage.

To test our model under different boundary conditions, we performed a measurement during which the amplitude of the step stress acting on the cell surface was varied. Within this measurement, the laser power is chosen randomly for each cell, viz 0.5, 0.6, 0.7 or 0.8 W, respectively. This procedure guaranteed that all other conditions, except for the power and hence the heat development in the μOS, remained constant. The strain is fitted with Eq. (4) as described above. As expected, the strain increases with increasing laser power; hence, the fit parameters a_1, a_2 and b_1 vary significantly between the fits. Figure 6 shows the activity parameter A of this measurement. As reported earlier, the TRPV1 channel opening probability rises at temperatures produced by laser powers close to 0.7 W (Gyger et al. 2011). At 0.5 W, more than 30 % of the strains can be fitted with an activity parameter close to zero (Fig. 6a). With increasing laser power, this fraction of non-active cells decreases (Fig. 6b–d). At 0.8 W, the fraction of passively elongating cells drops to approximately 16 %.

Discussion

Mechanisms of cellular contractions

In search of the origin of whole-cell contractions, force-generating processes on the molecular scale have to be considered. While polymerization processes such as actin treadmilling can cause protrusions (Ridley et al. 2003; Mogilner and Keren 2009), depolymerization processes and molecular motors can cause contractile forces. Contractions induced by myosin motors have been the focus of

many studies investigating cellular activity (Beningo et al. 2006; Wysolmerski and Lagunoff 1990; Bendix et al. 2008; Liverpool et al. 2009). The main activation of smooth muscular and non-muscular myosin happens via a Ca^{2+}-dependent pathway: Ca^{2+} binds to calmodulin, forming a Ca^{2+}/calmodulin complex that activates myosin light chain kinase (MLCK). The balance of MLCK, phosphorylating the myosin regulatory light chain, and myosin light chain phosphotase, dephosphorylating it, determines the activity of the myosin motors (Fukata et al. 2001; Somlyo and Somlyo 2003).

Blocking the Ca^{2+}-dependent myosin phosphorylation by inhibition of the MLCK with ML-7 leads to larger strains in HEK293-TRPV1 but not in wild-type cells. Hence, Ca^{2+}-dependent myosin activation plays a role in the generation of the contractions. This is in agreement with previous findings in measurements using attached beads (Kollmannsberger et al. 2011). However, we show that the contractions are not completely inhibited by ML-7. Furthermore, suppressing internal Ca^{2+} signaling or blocking Ca^{2+} influx showed an independent influence on the strain. Myosin seems not to be the only mechanism leading to contractions in suspended HEK293-TRPV1 cells.

Magnetic tweezer experiments with beads attached to the cytoskeleton have confirmed that the Ca^{2+}-dependent myosin activation plays a role in the generation of the contractions (Kollmannsberger et al. 2011). Our results show that suppressing internal Ca^{2+} signaling and blocking Ca^{2+} influx have a significant influence on the strain but do not inhibit the contractions entirely. This finding shows that contractions in the investigated cells are triggered via more than one mechanism. It has to be mentioned in this context that BAPTA does not deplete Ca^{2+} inside the cells, but competitively binds the Ca^{2+} ions, such that the probability to participate in signaling cascades is drastically reduced. Fluorescence Ca^{2+} imaging shows that the Ca^{2+} concentration rises during the experiment, as it does not reach the Ca^{2+} pumps transporting it out of the cell soma (Gyger et al. 2011).

Calcium-regulated actin-modifying proteins, such as villin, gelsolin and severin, can lead to Ca^{2+}-induced actin depolymerization (Walsh et al. 1984; Kumar et al. 2004; Larson et al. 2005) and could lead to contractions of the cell: Contractile forces arise from enthalpic contributions of attractive interactions; on the other hand, entropic contributions to the free energy favor a spread of the material, giving rise to a pressure that acts to expand the volume. A cross-linked network, such as the cytoskeleton, reaches an equilibrium density if these two contributions are balanced. Under the condition that monomers are able to diffuse away, a depolymerization, for example, driven by the Ca^{2+} influx, reduces the filament density, and the system contracts to reestablish the preferred density (Sun et al. 2010).

Moreover, microtubules could be shown to depolymerize when exposed to free Ca^{2+} (Salmon and Segall 1980). On one hand this directly causes a considerable amount of force (Grishchuk et al. 2005; Molodtsov et al. 2007). On the other hand, following the assumptions of the tensegrity model, microtubules provide the structures that resist the cellular pre-stress (Ingber 1997; Wang et al. 2001b). Depolymerization of microtubles would, according to this model, also cause contractions of the cell. As myosin contractility provides the contractile part of tensegrity, this model would also suggest that there are myosin-dependent and -independent effects on the contractility.

In plate rheological studies, contractile forces could be shown to arrise from the cell spreading, including slow building of actin stress fibers as a response to subtrate stiffness (Thoumine and Ott 1997). This process depends on cellular adhesions and happens on the order of hundreds of seconds. Obviously, the effect in our experiments, a fast, adhesion-independent contraction partially triggered by Ca^{2+}, does not originate from the same mechanisms.

While our phenomenological model does not give direct access to the microscopic origins of contractions, it allows classifying the influence of different mechanisms in an unbiased way. As shown for the second messenger Ca^{2+} and inhibition of Ca^{2+}-dependent myosin activation, the influence of different pathways possibly leading to contractions can be targeted in combination with adequate drugs. Ca^{2+}-independent inhibition of myosin by blebbistatin, disrupting or stabilizing actin filaments by cytochalasins and jasplakinolide or microtubules by nocodazole and taxol are experiments that can further elucidate the influence of the named mechanisms. In this way, our method for analyzing the data provides a powerful tool to judge the influence of specific molecular processes on cellular contractions.

Applicability of the model

We derive a descriptive model for cellular strain upon external stress that incorporates an active reaction of the cell. Approximating the constitutive equation (Eq. 2) by the leading terms of the Taylor expansion allows solving the problem analytically.

Reconstituted systems consisting of cross-linked biopolymers show a pronounced stress-stiffening response under deformation, if filament density, cross-linker concentration, or filament stiffness is high enough (Gardel et al. 2004; Xu et al. 2000). In composite materials such as cross-linked F-actin networks with small concentration of microtubules (Lin et al. 2011) or in the presence of active molecular motors (Mizuno et al. 2007; Broedersz and

MacKintosh 2011), these non-linear effects have been shown even to be enhanced. Living cells were demonstrated to show non-linear effects when measured with microplate rheology (Fernández et al. 2006; Fernández and Ott 2008) and magnetic twisting cytometry (Kollmannsberger et al. 2011; Wang et al. 1993). In this context, it is even more surprising that our simple phenomenological model with a linear approximation of the active stress term and up to second order terms in the stress-strain relation is able to describe the behavior of cells in the μOS. The data presented in this work show that this simple approach allows identifying active cells and quantifying the degree of activity without biasing the view by assumptions about the molecular mechanisms.

The reason for the applicability of a linear approximation for our experiments is most likely the small strain of maximally 6 % (Fig. 1). Furthermore, experiments of Wang et al. show that only force application to beads specifically bound to β_1 integrins result in a stress stiffening, whereas those bound to receptors that do not contribute to focal adhesion formation did not (Wang et al. 1993). In the μOS, forces are continuously distributed over the surface and do not act on discrete binding sites as in attached beads. Local strain variation is hence expected to be much less than in experiments with bound beads.

On the time scale of 5 s, as in the presented experiments, breakage of cross-links and hence plastic effects cannot be avoided completely. At a close look at times slightly below $t = 5$ s, Fig. 4 shows that the fitting gets worse toward the end of the stretch phase. These circumstances are accounted for by weighting the fit with the inverse square of the interquartile distance. While the model holds true for the time scales observed in this work, it will break down for longer experiments.

As discussed earlier, the assumption that the active cellular force ceases immediately when the external stress is switched off turns out to be too strong. The material does not relax passively when external stress application is terminated. Incorporation of this finding into our mathematical model would, however, require knowledge about the type of decay of the forces exerted by the cell after the end of the external stress application. To this end, at least one more parameter has to be identified and introduced in the model.

For some cells the measured strain is of the order of the uncertainty of the algorithm that detects the cell's edge. It can be assumed that in these cells the external and internal stress compensate each other at the beginning of the stretch phase. For these cases, fitting leads to diverging parameters (Fig. S7 in the ESM). A second reason that causes diverging parameters is a local minimum in the strain that occurs several seconds after the start of the experiment. This minimum indicates that the force exerted by the cell on its surface is not constantly increasing as assumed, but potentially decays after several seconds. The external stress then causes a strain with a positive derivative toward the end of the stretch. To overcome this problem, we weight the measured strain values in the fitting with the inverse square of the time-dependent interquartile distance of the measured strain distribution. The interquartile distance is increasing with time of stretching because of an increasing spread of the measured strain values. This approach leads to more accurate fits at the beginning and a larger deviation between theoretical and measured strain toward the end. While it results in convergence of the fit parameters for most of the cells, for some of the measured strain curves, the deviation is still too strong, and the fitting does not converge. Nevertheless, for most of the measured cells (88.5 %), our description with the leading term of contractile forces is sufficient to distinguish active from non-active cells and to quantify the activity.

Strain distributions

Optical Stretcher experiments with C2C12 myoblasts, a muscle precursor cell line, and cultured HMEC, a human breast cancer cell from primary tissue, reveal similar cellular contractions (data not shown), confirming that we are reporting on a real effect. In contrast, experiments with Balb3t3 fibroblasts show a strong internal Ca^{2+}-release upon Optical Stretching that does not result in contractions (data not shown). Hence, the effect seems to be caused by a cell-type-specific mechanism that is not present in fibroblasts.

The incorporation of an active term into the description of cell mechanics, as presented in this work, delivers an explanation concerning why suspended cells do not generally follow the power-law rheological predictions. Most of the 2-s μOS experiments do not lead to visible contractions (Wottawah et al. 2005a, b; Guck et al. 2005). However, when observed for 5 s as in the presented experiments, contractions become obvious. Our results predict an early onset of these contractions leading to a deviation from any expected passive modeling even when contractions do not become visible for shorter observation times. In a creep rheology measurement in the μOS at 0.7 W per fiber for 5 s, the deformation of only 18 % of the measured HEK293-TRPV1 cells and 22 % of the wild-type cells could be described by a passive viscoelasticity. This finding reveals that contractility has a major influence on cell rheology and cannot be neglected.

While in the first papers about the μOS, Gaussian distributions were fitted to the data (Guck et al. 2005), recent measurements of cell rheology with other methods have shown that if power-law rheology applies, the strain

follows a log-normal distribution (Fabry et al. 2001; Hoffman et al. 2006). Our results reveal changes of the actual distribution even for one cell type when pathways controlling the activity of the cells are manipulated. While the untreated HEK293-TRPV1 cells exhibit a sightly negative skewness in their strain distribution, the distributions with blocked Ca^{2+} tend to have a positive skewness. We therefore propose that the origin of part of the distribution's skewness lies in the intrinsic activity of the cells. Also subpopulations within measured cell lines and especially in primary cells should lead to skewed distributions. This will, in general, depend on the cell type and on the drug application. The absence of a general distribution describing the results of all of the measurements complicates the statistical analysis of the data. The Wilcoxon rank sum test (Mann and Whitney 1947) is a non-parametric possibility to test for the hypothesis that two distributions are equal. Calculating the CI with bootstrapping (Efron and Tibshirani 1994) can help to judge whether two medians differ significantly.

Conclusions

Mechanical properties of cells in response to external forces and stimuli are the result of passive and active cellular behavior. We observe contractions in single suspended epithelial cells against a stress externally applied by the Optical Stretcher. The use of a cell line transfected with a temperature-sensitive ion channel as a model system allows investigating the mechanics of cells in which a massive Ca^{2+} influx is triggered during the measurement. These experiments reveal an involvement of the second messenger Ca^{2+} in the pathway of the contractions in suspended cells.

We present a phenomenological mathematical model including a term accounting for active cellular stresses and show that this approach allows quantifying the contractions and distinguishing between active and non-active cells. We furthermore observe that the strain of active cells does not follow a fixed general distribution but depends on the activity of the cells. This complicates statistical analysis as appropriate tests for significance have to be found for every experiment. The introduced model reveals an influence of contractility even in measurements that seemingly can be described with passive viscoelastic approaches. Ignoring these contractions might lead to misinterpretation and erroneous material properties. On the other hand, a better understanding of contractile processes in cells might pave the way for better mechanical phenotyping of cells in future investigations and have important implications for new approaches in medical diagnosis and therapies.

Acknowledgments We thank B. Fabry (Friedrich Alexander University of Erlangen-Nürnberg) for helpful discussions and advice. Furthermore, we thank D. Julius (UCSF) for providing the TRPV1 transfected HEK293 cells. The project was funded by SAB-project 13403 (EFRE) and Agescreen-Biophotonics 5 Program [funded by the German Federal Ministry of Education and Research (BMBF)] and the graduate school Leipzig School of Natural Sciences—Building with Molecules and Nano-objects "BuildMoNa" of the Universität Leipzig.

References

Ananthakrishnan R, Guck J, Wottawah F, Schinkinger S, Lincoln B, Romeyke M, Käs J (2005) Modelling the structural response of an eukaryotic cell in the Optical Stretcher. Curr Sci India 88(9):1434–1440

Bement WM, Forscher P, Mooseker MS (1993) A novel cytoskeletal structure involved in purse string wound closure and cell polarity maintenance. J Cell Biol 121(3):565–578. doi:10.1083/jcb.121.3.565

Bendix PM, Koenderink GH, Cuvelier D, Dogic Z, Koeleman BN, Brieher WM, Field CM, Mahadevan L, Weitz DA (2008) A quantitative analysis of contractility in active cytoskeletal protein networks. Biophys J 94(8):3126–3136. doi:10.1529/biophysj.107.117960

Beningo KA, Hamao K, Dembo M, Wang YL, Hosoya H (2006) Traction forces of fibroblasts are regulated by the Rho-dependent kinase but not by the myosin light chain kinase. Arch Biochem Biophys 456(2):224–231. doi:10.1016/j.abb.2006.09.025

Broedersz CP, MacKintosh FC (2011) Molecular motors stiffen non-affine semiflexible polymer networks. Soft Matter 7(7):3186–3191. doi:10.1039/C0SM01004A

Caterina M, Schumacher M, Tominaga M, Rosen T, Levine J, Julius D (1997) The capsaicin receptor: a heat-activated ion channel in the pain pathway. Nature 389(6653):816–824

Caterina MJ, Rosen TA, Tominaga M, Brake AJ, Julius D (1999) A capsaicin-receptor homologue with a high threshold for noxious heat. Nature 398(6726):436–441

Cates ME, MacKintosh FC (2011) Active soft matter. Soft Matter 7(7):3050–3051. doi:10.1039/C1SM90014E

Desprat N, Richert A, Simeon J, Asnacios A (2005) Creep function of a single living cell. Biophys J 88(3):2224–2233. doi:10.1529/biophysj.104.050278

Efron B, Tibshirani RJ (1994) An introduction to the bootstrap. Chapman & Hall/CRC Monographs on statistics and applied probability. Taylor & Francis, London. http://books.google.de/books?id=gLlpIUxRntoC

Fabry B, Maksym GN, Butler JP, Glogauer M, Navajas D, Fredberg JJ (2001) Scaling the microrheology of living cells. Phys Rev Lett 87(14):148102. doi:10.1103/PhysRevLett.87.148102

Fernández P, Ott A (2008) Single cell mechanics: stress stiffening and kinematic hardening. Phys Rev Lett 100(23):238102. doi:10.1103/PhysRevLett.100.238102

Fernández P, Pullarkat PA, Ott A (2006) A master relation defines the nonlinear viscoelasticity of single fibroblasts. Biophys J 90(10):3796–3805. doi:10.1529/biophysj.105.072215

Friedl P, Gilmour D (2009) Collective cell migration in morphogenesis, regeneration and cancer. Nat Rev Mol Cell Bio 10(7):445–457

Fritsch A, Höckel M, Kiessling T, Nnetu KD, Wetzel F, Zink M, Käs JA (2010) Are biomechanical changes necessary for tumour progression? Nat Phys 6(10):730–732

Fukata Y, Kaibuchi K, Amano M, Kaibuchi K (2001) Rho–Rho-kinase pathway in smooth muscle contraction and cytoskeletal reorganization of non-muscle cells. Trends Pharmacol Sci 22(1):32–39. doi:10.1016/S0165-6147(00)01596-0

Gardel ML, Shin JH, MacKintosh FC, Mahadevan L, Matsudaira P, Weitz DA (2004) Elastic behavior of cross-linked and bundled actin networks. Science 304(5675):1301–1305. doi:10.1126/science.1095087

Grishchuk EL, Molodtsov MI, Ataullakhanov FI, McIntosh JR (2005) Force production by disassembling microtubules. Nature 438(7066):384–388

Guck J, Schinkinger S, Lincoln B, Wottawah F, Ebert S, Romeyke M, Lenz D, Erickson HM, Ananthakrishnan R, Mitchell D, Käs J, Ulvick S, Bilby C (2005) Optical deformability as an inherent cell marker for testing malignant transformation and metastatic competence. Biophys J 88(5):3689–3698. doi:10.1529/biophysj.104.045476

Gyger M, Rose D, Stange R, Kießling T, Zink M, Fabry B, Käs JA (2011) Calcium imaging in the Optical Stretcher. Opt Express 19(20):19212–19222. doi:10.1364/OE.19.019212

Hoffman BD, Massiera G, Van Citters KM, Crocker JC (2006) The consensus mechanics of cultured mammalian cells. Proc Natl Acad Sci USA 103(27):10259–10264. doi:10.1073/pnas.0510348103

Icard-Arcizet D, Cardoso O, Richert A, Hénon S (2008) Cell stiffening in response to external stress is correlated to actin recruitment. Biophys J 94(7):2906–2913. doi:10.1529/biophysj.107.118265

Ingber DE (1997) Tensegrity: the architectural basis of cellular mechanotransduction. Annu Rev Physiol 59(1):575–599. doi:10.1146/annurev.physiol.59.1.575

Jacinto A, Wood W, Balayo T, Turmaine M, Martinez-Arias A, Martin P (2000) Dynamic actin-based epithelial adhesion and cell matching during Drosophila dorsal closure. Curr Biol 10(22):1420–1426. doi:10.1016/S0960-9822(00)00796-X

Jonas O, Mierke CT, Käs JA (2011) Invasive cancer cell lines exhibit biomechanical properties that are distinct from their noninvasive counterparts. Soft Matter 7(24):11488–11495. doi:10.1039/C1SM05532A

Kollmannsberger P, Mierke CT, Fabry B (2011) Nonlinear visco-elasticity of adherent cells is controlled by cytoskeletal tension. Soft Matter 7(7):3127–3132. doi:10.1039/C0SM00833H

Kumar N, Tomar A, Parrill AL, Khurana S (2004) Functional dissection and molecular characterization of calcium-sensitive actin-capping and actin-depolymerizing sites in villin. J Biol Chem 279(43):45036–45046. doi:10.1074/jbc.M405424200

Larson L, Arnaudeau S, Gibson B, Li W, Krause R, Hao B, Bamburg JR, Lew DP, Demaurex N, Southwick F (2005) Gelsolin mediates calcium-dependent disassembly of Listeria actin tails. Proc Natl Acad Sci USA 102(6):1921–1926. doi:10.1073/pnas.0409062102

Lau AWC, Hoffman BD, Davies A, Crocker JC, Lubensky TC (2003) Microrheology, stress fluctuations, and active behavior of living cells. Phys Rev Lett 91(19):198101. doi:10.1103/PhysRevLett.91.198101

Lin YC, Koenderink GH, MacKintosh FC, Weitz DA (2011) Control of non-linear elasticity in F-actin networks with microtubules. Soft Matter 7(3):902–906

Lincoln B, Schinkinger S, Travis K, Wottawah F, Ebert S, Sauer F, Guck J (2007) Reconfigurable microfluidic integration of a dual-beam laser trap with biomedical applications. Biomed Microdev 9(5):703–710

Liverpool TB, Marchetti MC, Joanny JF, Prost J (2009) Mechanical response of active gels. Europhys Lett 85(1):18007

Lo CM, Buxton DB, Chua GC, Dembo M, Adelstein RS, Wang YL (2004) Nonmuscle myosin IIB is involved in the guidance of fibroblast migration. Mol Biol Cell 15(3):982–989. doi:10.1091/mbc.E03-06-0359

Lo CM, Wang HB, Dembo M, Wang YL (2000) Cell movement is guided by the rigidity of the substrate. Biophys J 79(1):144–152. doi:10.1016/S0006-3495(00)76279-5

Lodish H (2000) Molecular cell biology. W.H. Freeman and Company, New York

MacKintosh FC, Levine AJ (2008) Nonequilibrium mechanics and dynamics of motor-activated gels. Phys Rev Lett 100(1):018104. doi:10.1103/PhysRevLett.100.018104

Mader CC, Hinchcliffe EH, Wang YL (2007) Probing cell shape regulation with patterned substratum: requirement of myosin II-mediated contractility. Soft Matter 3(3):357–363. doi:10.1039/B606590B

Maloney JM, Nikova D, Lautenschläger F, Clarke E, Langer R, Guck J, Vliet KJV (2010) Mesenchymal stem cell mechanics from the attached to the suspended state. Biophys J 99(8):2479–2487. doi:10.1016/j.bpj.2010.08.052

Mann HB, Whitney DR (1947) On a test of whether one of two random variables is stochastically larger than the other. Ann Math Statist 18(1):50–60

Martin AC, Kaschube M, Wieschaus EF (2009) Pulsed contractions of an actin-myosin network drive apical constriction. Nature 457(7228):495–499

Mierke CT, Rösel D, Fabry B, Brábek J (2008) Contractile forces in tumor cell migration. Eur J Cell Biol 87(8–9):669–676. doi:10.1016/j.ejcb.2008.01.002

Mitrossilis D, Fouchard J, Guiroy A, Desprat N, Rodriguez N, Fabry B, Asnacios A (2009) Single-cell response to stiffness exhibits muscle-like behavior. Proc Natl Acad Sci USA 106(43):18243–18248. doi:10.1073/pnas.0903994106

Mizuno D, Tardin C, Schmidt CF, MacKintosh FC (2007) Nonequilibrium mechanics of active cytoskeletal networks. Science 315(5810):370–373. doi:10.1126/science.1134404

Mogilner A, Keren K (2009) The shape of motile cells. Curr Biol 19(17):R762–R771. doi:10.1016/j.cub.2009.06.053

Mogilner A, Oster G (2003) Force generation by actin polymerization II: the elastic ratchet and tethered filaments. Biophys J 84(3):1591–1605

Molodtsov M, Grishchuk E, McIntosh J, Ataullakhanov F (2007) Measurement of the force developed by disassembling microtubule during calcium-induced depolymerization. Dokl Biochem Biophys 412(1):18–21

Munevar S, Wang YL, Dembo M (2001) Traction force microscopy of migrating normal and H-ras transformed 3T3 fibroblasts. Biophys J 80(4):1744–1757. doi:10.1016/S0006-3495(01)76145-0

Park SW, Schapery RA (1999) Methods of interconversion between linear viscoelastic material functions. Part I–a numerical method based on Prony series. Int J Solids Struct 36(11):1653–1675. doi:10.1016/S0020-7683(98)00055-9

Pelham RJ, Wang YL (1999) High resolution detection of mechanical forces exerted by locomoting fibroblasts on the substrate. Mol Biol Cell 10(4):935–945

Remmerbach TW, Wottawah F, Dietrich J, Lincoln B, Wittekind C, Guck J (2009) Oral cancer diagnosis by mechanical phenotyping. Cancer Res 69(5):1728–1732. doi:10.1158/0008-5472.CAN-08-4073

Ridley AJ, Schwartz MA, Burridge K, Firtel RA, Ginsberg MH, Borisy G, Parsons JT, Horwitz AR (2003) Cell migration: Integrating signals from front to back. Science 302(5651):1704–1709. doi:10.1126/science.1092053

Saitoh M, Ishikawa T, Matsushima S, Naka M, Hidaka H (1987) Selective inhibition of catalytic activity of smooth muscle myosin light chain kinase. J Biol Chem 262(16):7796–7801

Salmon ED, Segall RR (1980) Calcium-labile mitotic spindles isolated from sea urchin eggs (*Lytechinus variegatus*). J Cell Bio 86(2):355–365. doi:10.1083/jcb.86.2.355

Somlyo AP, Somlyo AV (2003) Ca^{2+} sensitivity of smooth muscle and nonmuscle myosin II: modulated by g proteins, kinases, and myosin phosphatase. Physiol Rev 83(4):1325–1358. doi:10.1152/physrev.00023.2003

Stamenovic D, Suki B, Fabry B, Wang N, Fredberg JJ, Buy JE (2004) Rheology of airway smooth muscle cells is associated with cytoskeletal contractile stress. J Appl Physiol 96(5):1600–1605. doi:10.1152/japplphysiol.00595.2003

Sun SX, Walcott S, Wolgemuth CW (2010) Cytoskeletal cross-linking and bundling in motor-independent contraction. Curr Biol 20(15):R649–R654. doi:10.1016/j.cub.2010.07.004

Tamada M, Perez TD, Nelson WJ, Sheetz MP (2007) Two distinct modes of myosin assembly and dynamics during epithelial wound closure. J Cell Biol 176(1):27–33. doi:10.1083/jcb.200609116

Thoumine O, Ott A (1997) Time scale dependent viscoelastic and contractile regimes in fibroblasts probed by microplate manipulation. J Cell Sci 110(17):2109–2116

Tominaga M, Caterina MJ, Malmberg AB, Rosen TA, Gilbert H, Skinner K, Raumann BE, Basbaum AI, Julius D (1998) The cloned capsaicin receptor integrates multiple pain-producing stimuli. Neuron 21(3):531–543. doi:10.1016/S0896-6273(00)80564-4

Tschoegl NW (1989) The phenomenological theory of linear viscoelastic behavior. Springer-Verlag, New York

Vicente-Manzanares M, Ma X, Adelstein RS, Horwitz AR (2009) Non-muscle myosin II takes centre stage in cell adhesion and migration. Nat Rev Mol Cell Bio 10(11):778–790

Walsh TP, Weber A, Davis K, Bonder E, Mooseker M (1984) Calcium dependence of villin-induced actin depolymerization. Biochemistry (US) 23(25):6099–6102. doi:10.1021/bi00320a030

Wang N, Butler J, Ingber D (1993) Mechanotransduction across the cell surface and through the cytoskeleton. Science 260(5111):1124–1127. doi:10.1126/science.7684161

Wang HB, Dembo M, Hanks SK, Wang Yl (2001a) Focal adhesion kinase is involved in mechanosensing during fibroblast migration. Proc Natl Acad Sci USA 98(20):11295–11300. doi:10.1073/pnas.201201198

Wang N, Naruse K, Stamenović D, Fredberg JJ, Mijailovich SM, Tolić-Norrelykke IM, Polte T, Mannix R, Ingber DE (2001b) Mechanical behavior in living cells consistent with the tensegrity model. Proc Natl Acad Sci USA 98(14):7765–7770. doi:10.1073/pnas.141199598

Wei C, Wang X, Chen M, Ouyang K, Song LS, Cheng H (2009) Calcium flickers steer cell migration. Nature 457(7231):901–905

Wottawah F, Schinkinger S, Lincoln B, Ananthakrishnan R, Romeyke M, Guck J, Käs J (2005a) Optical rheology of biological cells. Phys Rev Lett 94(9):098103. doi:10.1103/PhysRevLett.94.098103

Wottawah F, Schinkinger S, Lincoln B, Ebert S, Müller K, Sauer F, Travis K, Guck J (2005b) Characterizing single suspended cells by optorheology. Acta Biomater 1(3):263–271. doi:10.1016/j.actbio.2005.02.010

Wysolmerski RB, Lagunoff D (1990) Involvement of myosin light-chain kinase in endothelial cell retraction. Proc Natl Acad Sci USA 87(1):16–20

Xu J, Tseng Y, Wirtz D (2000) Strain hardening of actin filament networks. J Biol Chem 275(46):35886–35892. doi:10.1074/jbc.M002377200

Yamada S, Wirtz D, Kuo SC (2000) Mechanics of living cells measured by laser tracking microrheology. Biophys J 78(4):1736–1747. doi:10.1016/S0006-3495(00)76725-7

Yeung T, Georges PC, Flanagan LA, Marg B, Ortiz M, Funaki M, Zahir N, Ming W, Weaver V, Janmey PA (2005) Effects of substrate stiffness on cell morphology, cytoskeletal structure, and adhesion. Cell Motil Cytoskel 60(1):24–34. doi:10.1002/cm.20041